Thin Fresnel Zone Plate Lenses for Underwater Acoustics: Modeling and Experiments

David C. Calvo, Abel L. Thangawng, Michael Nicholas, Christopher N. Layman
Naval Research Laboratory, Acoustics Division, Code 7165,
Washington, DC 20375 USA

***Abstract*—In situations where size, weight, and system complexity are important, Fresnel zone plate (FZP) lenses have potential advantages in acoustic systems. Numerical modeling and laboratory characterization of focusing by a Soret type FZP lens are presented in this study. Both rubber foam and resonant air cavity designs are considered for the opaque zones. This study extends previous work by examining a wider range of incident field angles. Measurements of a higher-order focus, more narrow than the primary focus but with reduced gain, are also presented that compare favorably with modeling predictions. Comparison is also made between standard diffraction theory predictions (Fourier acoustics) and finite-element, oblique wave scattering simulations for the axisymmetric FZP geometry. The latter accounts for edge effects and acoustic penetration through the lens material, and predicts a higher focal gain for oblique plane wave insonification. Finally, the directivity of an FZP lens and hydrophone combination is compared with that of an ideal pressure sensitive disk of equivalent diameter to assess gain vs. side-lobe tradeoffs. Calculations demonstrate 10 dB reduction of the first sidelobe level using the FZP with a 15% main lobe broadening.**

I. Introduction

Acoustic lenses have been investigated in the past as an alternative to phased-array beamforming in underwater acoustical imaging systems in the near MHz frequency range [1]–[3]. As frequencies are reduced, acoustic lenses become bulky, and so thin lens alternatives have been pursued. In electromagnetic work (e.g., soft X-rays, microwaves), Fresnel zone plate (FZP) diffractive lenses have been used in situations where refractive focusing is difficult to achieve with conventional lenses or in situations where planar fabrication is advantageous [4]. Studies of acoustic diffractive lenses have been few, although blazed gratings have been examined for imaging [5]. Thin Fresnel lenses that resemble plano-convex lenses with phase-redundant thickness regions removed can be interpreted as FZPs with transparent gradual phase shifting zones. Stamnes *et al*. created an acrylic lens of this type for MHz frequencies by using a two-level phase discretization for each zone [6], [7]. Mori *et al.* also simulated an impedance matched (rubber) Fresnel lens of this type with gradual thickness variation in each zone [8]. More recently, Nakamura *et al.* [9] and Sato *et al.* [10] have examined different thin lens designs.

Recently, we have fabricated and characterized a thin (0.4 λ) underwater acoustic Soret type FZP lens with alternating transparent and opaque zones as shown in Fig. 1(a) [11]. Our work advanced upon modeling work done in [12] which predicted performance in an ideal geometry but did not include experiments. The binary FZP considered here and in [11] has a simple and flexible construction based on silicone rubber (PDMS) foam bonded to a thin PDMS substrate film. When insonified by a plane wave, diffracted and reflected waves form foci on both the transmission and reflection sides of the lens as shown in Fig. 1(b). The FZP lens was designed to form a focus at F=8.75 cm for a 200 kHz incident plane wave. Zone radii b_n as a function of wavelength λ and focal length F are given by [4]

$$b_n = \sqrt{n\lambda F + \left(\frac{n\lambda}{2}\right)^2} \,. \tag{1}$$

Laboratory measurements demonstrated that focusing was obtained at the diffraction limit corresponding to the Rayleigh resolution criterion. An ultra-thin (0.0067 λ) FZP was also designed and simulated that used sets of resonant air-ring cavities in a thin layer of PDMS to create opaque zones [11].

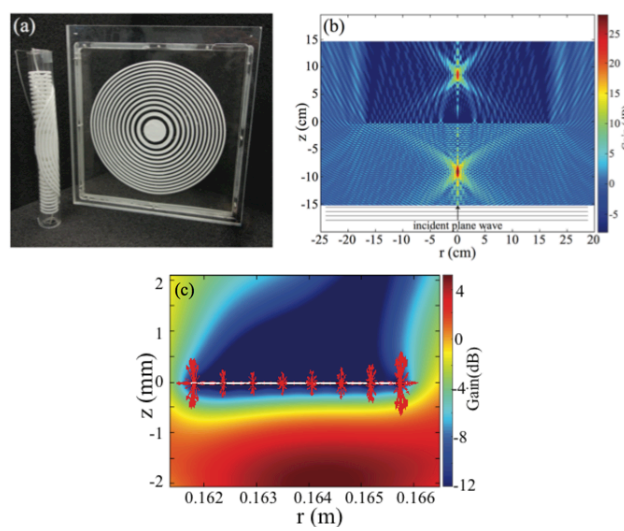

Fig. 1. (a) Fresnel zone plate lenses shown suspended in the test frame and coiled (lens diameter 13 inches). (b) FEM simulation of focusing on both the transmission and reflection sides of the rubber foam-based FZP insonified by a plane wave. The gain is defined as $20\log_{10}|p|$ for a unit amplitude plane wave in the z-direction. (c) Simulated gain field and resonant displacement vectors for the ultra-thin, pulsating air-ring cavity based design. The outermost opaque zone is displayed. Photograph and plots from [11].

Work sponsored by the Office of Naval Research.

In this paper, we expand on previous experimental results by considering wave incidence over wider angles than before. Comparison is also made between oblique incidence predictions using the classical theory of diffraction (i.e. Fourier acoustics) vs. the finite element method (FEM). Detailed measurements are also presented of a higher-order, narrow focusing feature compared to the main focus. Finally, focusing properties of the ultra-thin lens with air-ring cavities is also simulated for oblique incidence using an acoustic FEM. Comparison of FZP directivity is also made against the ideal situation of an equivalent diameter pressure sensitive disk.

II. Laboratory Measurements

A. Normal Incidence

Previous focusing results are summarized for convenience. Details of FZP fabrication and experimental methods can be found in [11]. Fig. 2 displays the transmitted pressure field for normal incidence for the rubber-foam based FZP in terms of a gain defined as $20\log_{10}|p_{\text{trans}}(r,z)/p_{\text{inc}}(0,0)|$. A 200 kHz piston source was used to insonify the FZP and a small hydrophone scanned the transmission side of the lens. The normalization value $p_{\text{inc}}(0,0)$ is the pressure amplitude at the position of the front face center of the lens but measured in the absence of the lens. This definition was used due to the geometrical decay of the pressure field from the piston compared to an ideal plane wave. The piston insonified a variable number of zones depending on separation from the lens. At 50 cm separation, the focal gain was 16.5 dB, while for 1 m separation the gain peaked at 20.3 dB. Axial shifting of the focus was caused by incident wavefront curvature. The finite-element computation modeled the rubber foam as a lossy fluid and accounted for piston insonification. Agreement between measurements and modeling were good over a large dynamic range, indicating that the fluid model for the opaque zones and PDMS substrate were adequate.

A noticeable feature in Fig. 2 not discussed in [11] is the higher-order narrow focus near $z=F/3$ which is caused by adding an additional wavelength to the interference condition that defines the zone radii [13]. For the primary focus at F=10.9 cm (for 1 m FZP-source separation), this higher-order focus is predicited at z=3.6 cm which agrees with the measurements shown in Fig 3. In judging the quality of a focus, different metrics are used in the literature. The classical Rayleigh expression is $r_{\text{Rayl}} = 0.61\lambda/\sin\theta_{\text{ap}}$ which is the radius from the main peak to first null in the Airy focal pattern [7]. This radius is used in the Rayleigh resolution criterion. The variable θ_{ap} is the angle between the aperture outermost edge and the axis of symmetry subtended from the focal spot of interest. This expression is useful in demonstrating the narrowing of the focus as the focal length is shortened ($\sin\theta_{\text{ap}}$ becomes closer to 1). An alternative is to use the expression for the full width at half maximum (FWHM). The higher-order focus has a FWHM = 0.65λ which is narrow but still above the conventional FWHM = 0.5λ ultimate limit for large aperture ($\sin\theta_{\text{ap}}$=1). The primary focus in comparison has FWHM = 0.86λ. The higher-order focal gain is 6.2 dB compared to 20.3 dB at the primary focus.

B. Oblique Incidence

As the angle of incidence is steered as shown in Fig. 4(a), the focus shifts much like a standard lens that creates an image of a source. Experimentally the incidence angle was changed by rotating and translating the piston source as shown in Fig. 4(b). The location of the focus can be determined using the construction in Fig. 4(c) for a dual of the FZP in which a direct path transmits through the center zone. This direct path must interfere constructively with diffracted waves through the peripheral zones [4], [12]. Fig. 4(a) shows that aberration is apparent since not all diffracted rays add in phase at the same location which leads to splitting of the focus into multiple peaks. While computing an average focal spot position from diffracted ray paths is possible, the simple geometric expression

$$\Delta x_F = F\tan\theta_{inc}\,, \tag{2}$$

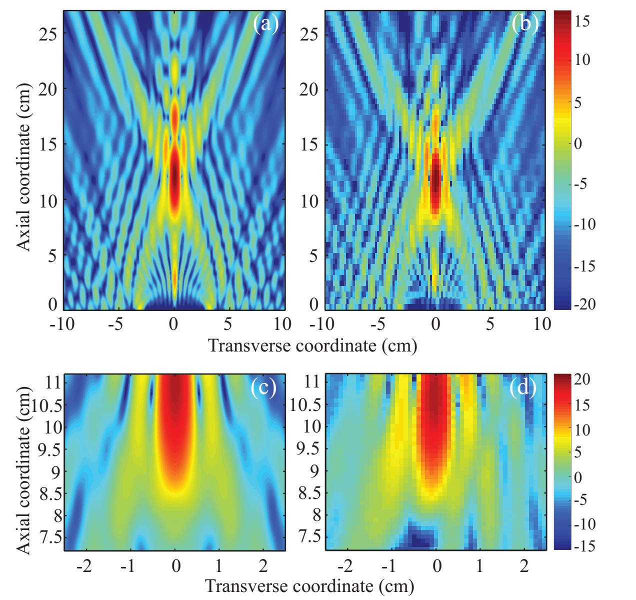

Fig. 2. FEM simulated (a,c) and measured (b,d) gains 20 log10$|p_{\text{trans}}/p_{\text{inc}}(0,0)|$ (dB) for 50 cm source-FZP separation (top row) and 1 m separation (bottom row). Piston insonification used. Gain is increased by insonifying more zones with a piston source. Figure from [11].

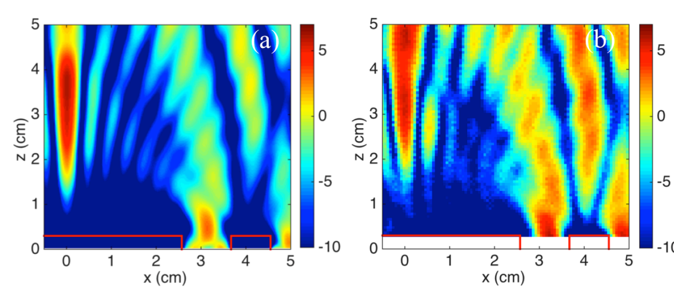

Fig. 3. FEM simulated (a) and measured (b) higher-order focus plotted as gain $20\log_{10}|p_{\text{trans}}/p_{\text{inc}}(0,0)|$ (dB). FZP-source separation is 1 m. Diffraction through first and second open annuli are visible.

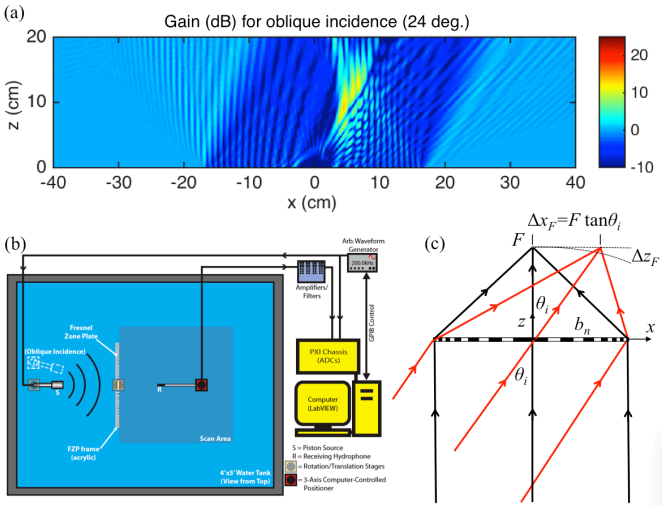

Fig. 4. (a) Calculation of transmitted field plotted in terms of gain $20\log_{10}|p_{total}|$ for an obliquely incident plane wave at 24°. (b) Schematic of experiment indicating sense of source rotation in the horizontal (*x,z*) plane. (c) Diffracted ray diagram indicating focal shift geometry (after [4], [12]).

which approximates the shift to be only transverse in the focal plane *z=F,* is a useful relation. Experimental and modeled focal plane results are shown in Fig. 5 for insonification with the piston transducer. The cross-pattern lines using Eq. 2 agree well with the measurements while the model overpredicts the shift.

III. Modeling for Oblique Incidence

Two approaches are followed for computationally efficient calculation of the transmitted field for oblique incidence. The first approach is classical diffraction theory formulated to make use of the FFT (Fourier acoustics) to compute the transmitted field given knowledge of the field at the aperture plane [14]. The second approach uses an axisymmetric finite element method (FEM) in which the oblique incident field is analytically decomposed into a number of axisymmetric Fourier modes that are compatible with the FZP axial symmetry. A series of axisymmetric scattering problems are then solved and the fields are summed to obtain the three-dimensional total field [15]. For simplicity, the modeling is restricted to a plane wave field and the rubber foam is modeled as a lossy fluid [11]. The FEM has the advantage of modeling the full interaction of the incident field with the edges of the FZP and within the aperture gaps that are bounded by the rubber foam. Due to the relatively short primary focal length, (θ_{ap} = 62°), a paraxial (narrow angle) approximation is of limited usefulness and is therefore not invoked in the modeling.

A. Fourier Acoustics

The standard Fourier acoustics radiation problem consists of a rigid plane (baffle) in which a distribution of normal acceleraton is specified over a finite area. Adaptation is necessary to the problem at hand in order to create the shadowing effects seen in the total acoustic pressure gain plots shown in Fig. 4(a). The approach is to begin with the inverse of the Fresnel zone plate mask (T) seen in Fig. 1(a). The pressure specified on the aperture plane is minus this mask times the incident pressure field which is assumed to be the field without the mask present:

$$p_0(x,y,0) = -T(x,y)\,p_{inc}(x,y,0). \tag{3}$$

The mask T has a value of 1 in the center disk and then alternates with 0 in the different Fresnel zones. Beyond the edge of the FZP, T=0. The pressure field is advanced to any z plane using the pressure propagator

$$p'_{trans}(x,y,0) = FT^{-1}\left\{FT\left\{p_0(x,y,0)\right\}\exp\left(i\sqrt{k^2-k_x^2-k_y^2}\,z\right)\right\}, \tag{4}$$

where FT denotes the two-dimensional Fourier transform, FT^{-1}

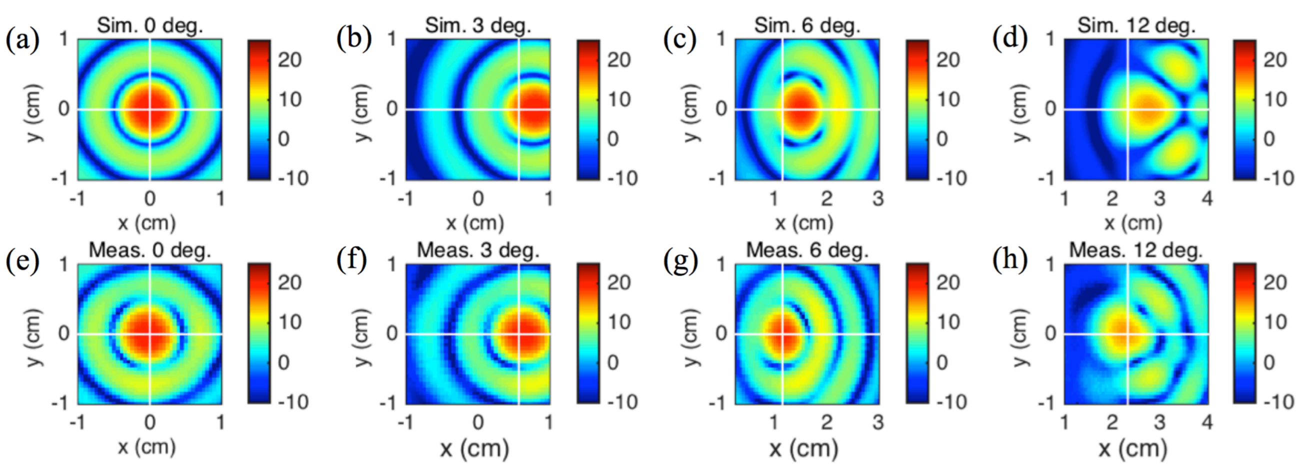

Fig. 5. Gain in the vertical focal plane for oblique insonification. Simulated (a)–(d) and measured (e)–(h) gain $20\log_{10}|p_{trans}(x,y,F)/p_{inc}(0,0,0)|$ (dB) in the peak focal planes F=11.0 cm (simulated) and F= 10.9 cm (experiment). Incidence angles θ_{inc} = 0, 3, 6, and 12 degrees for the four columns, respectively. Simulation computed using Fourier acoustics. Piston source incident field is used in both cases. The white cross is the focal shift relation $\Delta x_F = F\tan\theta_{inc}$.

its inverse, and k is the wavenumber in the water [14]. The total pressure field accounting for the shadows [shown in Fig. 4(a) for instance] is obtained by adding the incident field to the result

$$p_{total} = p'_{trans} + p_{inc} . \tag{5}$$

B. Axisymmetric FEM

The general technique for computing acoustic scattering from an axisymmetric elastic object is described by Zampolli *et al.* [15]. As a first step, we begin with a simpler model by approximating the FZP as an acoustic fluid since this proved adequate for the normal incidence results in Figs. 1 and 2. The FZP consists of lossy opaque zones (3 mm thick) with sound speed 272 m/s, density 680 kg/m^3, and attenuation 11.2 dB/wavelength. The lossy zones are bonded to a thin (1 mm) PDMS sheet of sound speed 1042 m/s and density 1020 kg/m^3. The water sound speed and density are 1482 m/s and 1000 kg/m^3, respectively.

The incident pressure field is decomposed into a Fourier series in polar-cylindrical coordinates (r, ϕ, z)

$$p_{inc}(r,\phi,z) = \sum_{m=0}^{\infty} \varepsilon_m p_m^{inc}(r,z)\cos(m\phi), \tag{6}$$

where ε_0=1 and ε_m=2 for m>0. For a plane wave, the individual (r,z) fields are given by

$$p_m^{inc}(r,z) = i^m e^{ikz\sin\theta_{inc}} J_m\left(kr\cos\theta_{inc}\right). \tag{7}$$

In the finite-element code used (COMSOL Multiphysics), each axisymmetric problem (with m as a parameter in the Helmholtz equation) consists of using (7) as an incident (background) field and truncating the domain using perfectly matched layers. The total scattered field is obtained by summing the scattered field solutions:

$$p_{scat}(r,\phi,z) = \sum_{m=0}^{\infty} \varepsilon_m p_m^{scat}(r,z)\cos(m\phi). \tag{8}$$

C. Modeling Results for Rubber Foam FZP

Comparison between Fourier acoustics (FA) and FEM results are presented in Fig. 6 (for ϕ=0, x=r). Generally the focal location and structure agree, although the FEM predicts a higher gain by about 4 dB when the incidence angle exceeds 3°. We note that plane wave incidence is assumed in these results and so care must be taken in comparing with results created using a piston incident field in Fig. 5. The simple expression (2) for focal shift remains accurate up to approximately 24°. For simplicity, the solution only for x>0 is plotted in the horizontal plane y=0. There is a significant difference in structure in the subdomain ($0 < x < 5$ cm , $0 < z < 5$ cm). This extends 7 wavelengths from the lens and is therefore not soley an evanescent near-field region. These observations are important if the higher-order focus in Fig. 3 must be resolved for oblique incidence.

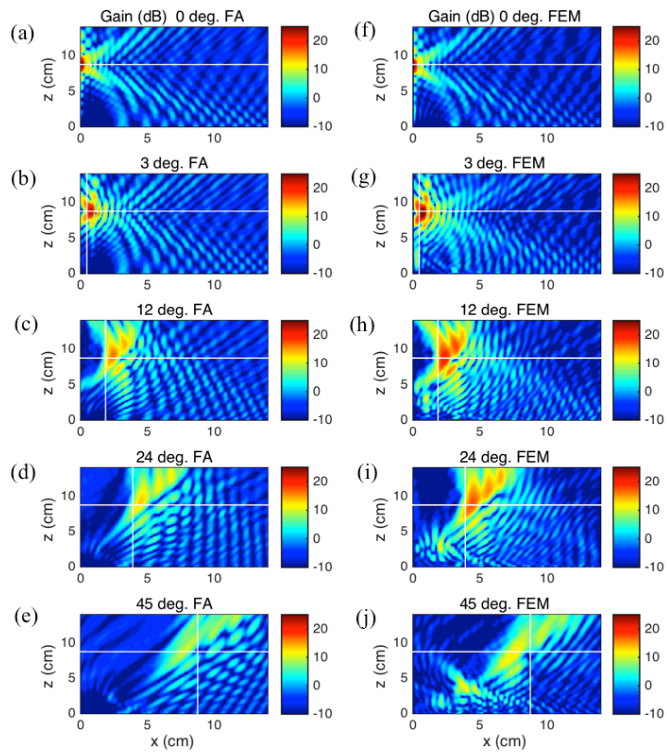

Fig. 6. Comparison of focusing behavior for obliquely incident plane waves calculated using Fourier acoustics (FA) [left column, (a) –(e)] and the FEM [right column, (f)–(j)]. Plane wave incidence angles θ_{inc} =0, 3, 12, 24, and 45 degrees for the five rows, respectively. Gain $20\log_{10}|p_{total}|$ is plotted.

D. Ultra-thin Resonant Cavity Case

In [11], an ultra-thin (0.0067λ) Soret type FZP was proposed and simulated that created opaque zones using sets of air-ring cavities inside a thin PDMS layer. The FZP was simulated only for normal incidence but made use of an acoustic-elastic model for its structure. While a model for oblique incidence would ideally use an axisymmetric elastic model, for simplicity we present results using a fluid model with the caveat that the resonance of the cavities could be significantly different for acoustic vs. elastic air cavities [16]. Although predicted focal levels could easily vary with an actual experiment, the calculation allows assessment of

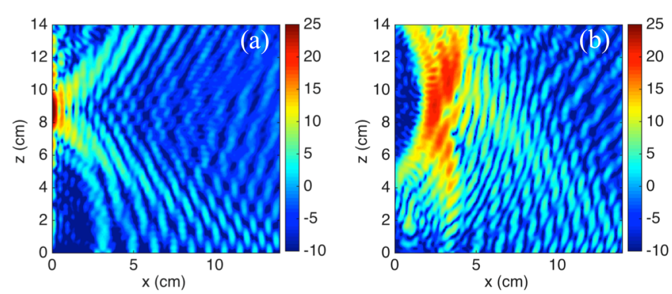

Fig. 7. Acoustic finite-element simulation of plane-wave focusing for an ultra-thin resonant air cavity-based FZP lens for 0° (a) and 12° (b) incidence angles. The ultra-thin geometry is reported in [11].

diffractive interference when the peripheral scatterers in a given opaque zone are resonantly oscillating with different phase (due to the oblique geometry) compared to the non-resonant rubber foam. The physics in this case is complex due to the collective effects of the air-ring oscillators in a given opaque zone, and so the FEM is particularly useful.

Results in Fig. 7 indicate that the focus is obtained at the anticipated position (F = 8.75 cm) for normal incidence. For 12° incidence, the transmitted field resembles the corresponding rubber-foam FEM result in Fig. 6(h) although the peaks in focal level in Fig. 7(b) have nearly identical level.

IV. Directivity Comparison

It is natural to compare the simulated directivity of the FZP considered with that of a pressure sensitive disk of the same diameter. The response of such a disk, assuming it could be uniformly constructed, is largest when the incident wave is at normal incidence since the compression of the layer would be uniform. It is important to note that although the disk responds most at normal incidence, it is not a lens, and would have to be mechanically steered to accomplish imaging.

In Fig. 8 we compare the directivity of a system comprised of the FZP with a single hydrophone at its focus vs. the directivity of the pressure sensitive disk. The disk directivity is computed simply by summing the pressure of the incident wave over its surface. Using the FZP, the first sidelobe is reduced by 10 dB with the main lobe -3 dB half-angle broadening from 0.64 to 0.74. The large difference in directivity as the angle is increased is due to the point hydrophone encountering an unattenuated plane wave as can be visualized in Fig. 4(a) as the incidence angle increases further.

V. Summary

Measurements have been presented that extend previous work by examining the higher-order focus in more detail as well as a wider range of incidence angles. The higher-order focus, being relatively closer to the lens, but more than a wavelength away, is naturally more narrow than the primary focus and has a FWHM = 0.65λ which is larger than the primary focus FWHM = 0.86λ. Measurements of focal shift for oblique wave incidence indicated that the simple imaging expression for transverse shift $z = F \tan\theta_{inc}$ agreed with the main lobe position. The Fourier acoustic result was accurate at predicting level although it overpredicted the focal shift. Comparison of the Fourier acoustics approach with the axisymmetric FEM acoustic scattering model demonstrated agreement with the focal shift and focal structure, although the FEM predicted significantly higher gain for a range of oblique plane wave angles. The exact cause of the focal shift discrepancy requires closer examination which could be done by accounting for full elastic effects in the axisymmetric FEM model.

Simple acoustic-only FEM modeling of the ultra-thin (resonant cavity) FZP lens for oblique incidence demonstated that focusing could still be obtained comparable to the rubber-foam FZP. Further analysis would require accounting for full elastic effects which thus far has only been included for normal incidence [11]. Finally, simple analysis of the difference between FZP directivity and that of an idealized pressure sensitive disk of equivalent diameter indicated a potential 10 dB sidelobe reduction using the FZP, although a more accurate comparison would use an elastic wave model for the disk (where the FZP could possibly exhibit more advantages). It is important to note, however, that the FZP lens is able to image (focal shift varies with incidence angle) whereas the pressure sensitive disk must be mechanically steered to create an image.

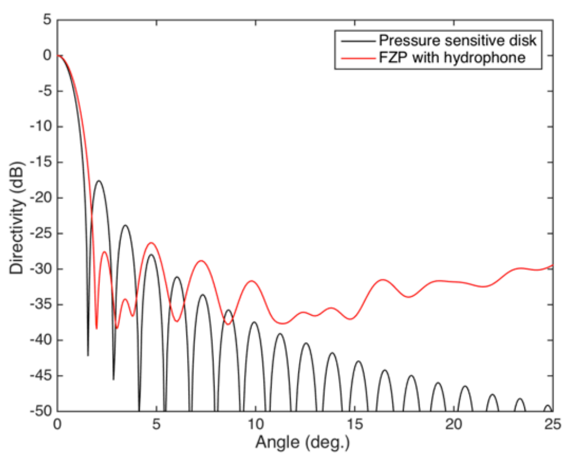

Fig. 8. Normalized directivity (dB) comparison between FZP and pressure sensitive disk both of 33 cm diameter (D = 45 λ at 200 kHz). Disk calculation is the sum of the oblique plane wave pressure distribution over the disk surface (flexural wave effects neglected). FZP result computed by Fourier acoustics as described in text.

References

[1] D.L. Folds, "Focusing properties of solid ultrasonic cylindrical lenses," *J. Acoust. Soc. Am.*, vol. 53, no. 3, pp. 826–834, 1973.

[2] D.L. Folds, "Status of ultrasonic lens development," in Underwater Acoustics and Signal Processing, *Proceedings of the NATO Advanced Study Institute*, Copenhagen, 18-19 August 1980, Boston: D. Reidel Publishing Compnay, 1980, pp. 263–279.

[3] E. Belcher, W. Hanot, and J. Burch, "Dual-frequency identification sonar (DIDSON)," in *Proceedings of the 2002 International Symposium on Underwater Technology*, Tokyo, Japan, April 2002, pp. 187–192.

[4] I.V. Minin and O.V. Minin, *Diffractional Optics of Millimetre Waves, Series on Optics and Optoelectronics*, Bristol, UK: CRC Press, 2004.

[5] R. L. Thompson, J. Seawall, and T. Josserand, "Two dimensional and three dimensional imaging results using blazed arrays," in *Proceedings of the OCEANS 2001 MTS/IEEE*, vol. 2, Honolulu, HI, USA, November 2001, pp. 985–988.

[6] J.J. Stamnes, T. Gravelsæter, and O. Bentsen, "Image quality and diffraction efficiency of a holographic lens for sound waves," in *Acoustical Imaging*, vol. 10, P. Alais and A. Metherell, Eds. New York: Plenum Press, 1982, pp. 587–606.

[7] J.J. Stamnes, *Waves in Focal Regions: Propagation, Diffraction and Focusing of Light, Sound and Water Waves*, Bristol, UK: CRC Press, 1986.

[8] K. Mori, A. Miyazaki, H. Ogasawara, T. Nakamura, and Y. Takeuchi, "Numerical analysis of sound pressure fields focused by phase continuous Fresnel lens using finite difference time domain method", *Jpn. J. Appl. Phys.*, part 1, vol. 46, 4990, July 2007.

[9] T. Nakamura, Y. Sato, H. Ogasawara, and K. Mitzutani, “Sound pressure field focused by doublet with acrylic plano-concave lens and silicon-rubber Fresnel lens,” in *Proc. MTS/IEEE OCEANS Conf.*, Bergen, Norway, June 2013.

[10] Y. Sato, K. Mizutani, N. Wakatsuki, and T. Nakamura, “Design for aplanatic Fresnel acoustic lens for underwater imaging,” *Jpn. J. Appl. Phys.*, part 1, vol. 48, 07GL04, July 2009.

[11] D.C. Calvo, A.L. Thangawng, M. Nicholas, and C.N. Layman, “Thin Fresnel zone plate lenses for focusing underwater sound,” *Appl. Phys. Lett.*, vol. 107, 014013, July 2015.

[12] W.J. Hughes and J.R. Craig, “The focusing properties of an acoustic thin lens and zone plate,” The Pennsylvania State University Applied Research Laboratory Technical Report No. TR96-003, April 1996.

[13] D. Attwood, *Soft X-Rays and Extreme Ultraviolet Radiation*, Cambridge, UK: Cambridge University Press, 1999.

[14] E.G. Williams, *Fourier Acoustics: Sound Radiation and Nearfield Acoustical Holography*, San Diego, CA: Academic Press, 1999.

[15] M. Zampolli, A. Tesei, F.B. Jensen, N. Malm, and J.B. Blottman III, “A computationally efficient finite element model with perfectly matched layers applied to scattering from axially symmetric objects,” *J. Acoust. Soc. Am.*, vol. 122, no. 3, pp. 1472–1485, June 2007.

[16] D.C. Calvo, A.L. Thangawng, and C.N. Layman, “Low-frequency resonance of an oblate spheroidal cavity in a soft elastic medium,” *J. Acoust. Soc. Am.*, vol. 132, no. 1, pp. EL1–EL7, July 2012.